Catalysis Today 167 (2011) 96–106

Contents lists available at ScienceDirect

Catalysis Today

journal homepage: www.elsevier.com/locate/cattod

Influence of alkali promoters on synthetic diesel production over Co catalyst

A.R. de la Osa[a,*], A. De Lucas[a], J.L. Valverde[a], A. Romero[a], I. Monteagudo[b], P. Coca[b], P. Sánchez[a]

[a] Chemical Engineering Department, Faculty of Chemistry, University of Castilla La Mancha, Avda. Camilo José Cela 12, 13071 Ciudad Real, Spain
[b] ELCOGAS, Carretera de Calzada Calatrava km 27, 13500 Puertollano, Spain

ARTICLE INFO

Article history:
Received 14 June 2010
Received in revised form 8 October 2010
Accepted 2 November 2010
Available online 3 January 2011

Keywords:
Fischer–Tropsch synthesis
Cobalt catalyst
Alkali-earth metal
Alkali metal

ABSTRACT

The effects of the addition of alkali metal and alkali-earth metal promoters over cobalt based catalyst on Fischer–Tropsch activity and on hydrocarbon product distribution were studied. The influence of promoters on the reducibility and cobalt particle size was studied by different techniques, including N_2 adsorption, X-ray diffraction, temperature-programmed reduction, temperature-programmed desorption and acid–base titrations. Experiments were carried out on a bench scale fixed bed reactor and catalysts were prepared by incipient wetness impregnation. It was observed that the addition of small amounts of these promoters (0.5 wt%) improved the cobalt oxide reducibility by reducing the formation of cobalt aluminate species. The interaction between cobalt oxide and promoted support was reduced and larger cobalt oxide particles were formed on the surface. A positive correlation between basicity and particle size was observed with the exception of K promoted sample. Furthermore, CO conversion and C_5^+ selectivity were found to be also influenced by the addition of promoters. An enhanced dispersion that provides abundant catalytically active sites was observed on promoted catalyst. The addition of Ca to the cobalt based catalyst greatly improved the diesel selectivity. However Ca promoted catalyst yield a higher amount of methane at 242 °C than the Na sample.

1. Introduction

Global warming has pushed the necessity to reduce the emissions of gases responsible for the Greenhouse effect, mainly CO_2, caused by the use of fossil fuels [1]. Coal gasification is a well established technology for producing syngas (CO and H_2) capable of being compatible with biomass and wastes as feedstock. The co-gasification of biomass with coal, could contribute to the reduction of the fossil fuels dependency and CO_2 emissions. Additional advantages related with the low ash and sulphur content of biomass have been reported by several authors [2]. ELCOGAS, located in Puertollano (Spain) is a coal and petcoke gasification central integrated with combined cycle, IGCC, with exemplary environmental characteristics. In a recent project the co-gasification of coal/petcoke and exhausted olive husk up to 10 wt% on the ELCOGAS IGCC plant has been demonstrated to be feasible for the production of a called biosyngas. Fischer–Tropsch synthesis (FTS) is a heterogeneously catalyzed polymerization process which converts syngas (CO and H_2) into hydrocarbons (liquid fuels). Thus, the transformation of biomass to liquid appears as an attractive alternative as a clean, renewable and sustainable energy source [3–5]. Water–gas shift reaction was usually proposed to increase the H_2/CO molar ratio close to 2 [6,7].

Among the potential FTS catalysts, such as ruthenium, nickel, iron and cobalt, only the last two appeared to be economically feasible at an industrial scale. Fe-based catalysts are considered to lead to more olefinic products and lower CH_4 selectivity than Co-based catalysts. Co-based catalysts are typically more active than Fe-based catalysts though they require lower reaction temperature [8]. Moreover, cobalt based catalysts were also widely used for FTS due to their high selectivity to linear paraffins, low water–gas shift activity and stability toward deactivation by water [9]. Some inorganic supports with high surface area such as silica and alumina have been used to increase the surface area of the cobalt. However, the formation of irreversible cobalt-aluminate during pretreatment and under reaction conditions decreased the catalytic activity due to the loss of active cobalt metal for catalyzing the reaction [10,11]. For alumina, the metal oxide–support interactions are stronger than other supports such as titania and silica [12]. In order to suppress these interactions, noble metals such as ruthenium [13] and rhenium [14] have been used as promoters. However, due to high prices, their industrial application is restricted. Thus, less expensive metal oxides have been investigated as promoters. It is known that the addition of some metal oxide promoters to cobalt catalysts could modify the support's texture, suppress the formation of cobalt-supported compounds and increase cobalt dispersion and reducibility.

There are numerous papers studying the influence of the addition of alkali promoters on FTS over iron-based catalysts [15,16]. However, literature related to alkali promoter effect on cobalt cat-

* Corresponding author. Tel.: +34 926 29 53 00x3509; fax: +34 926 29 52 56.
E-mail addresses: AnaRaquel.Osa@uclm.es, Anraqel@gmail.com (A.R. de la Osa).

0920-5861/$ – see front matter © 2010 Elsevier B.V. All rights reserved.
doi:10.1016/j.cattod.2010.11.064

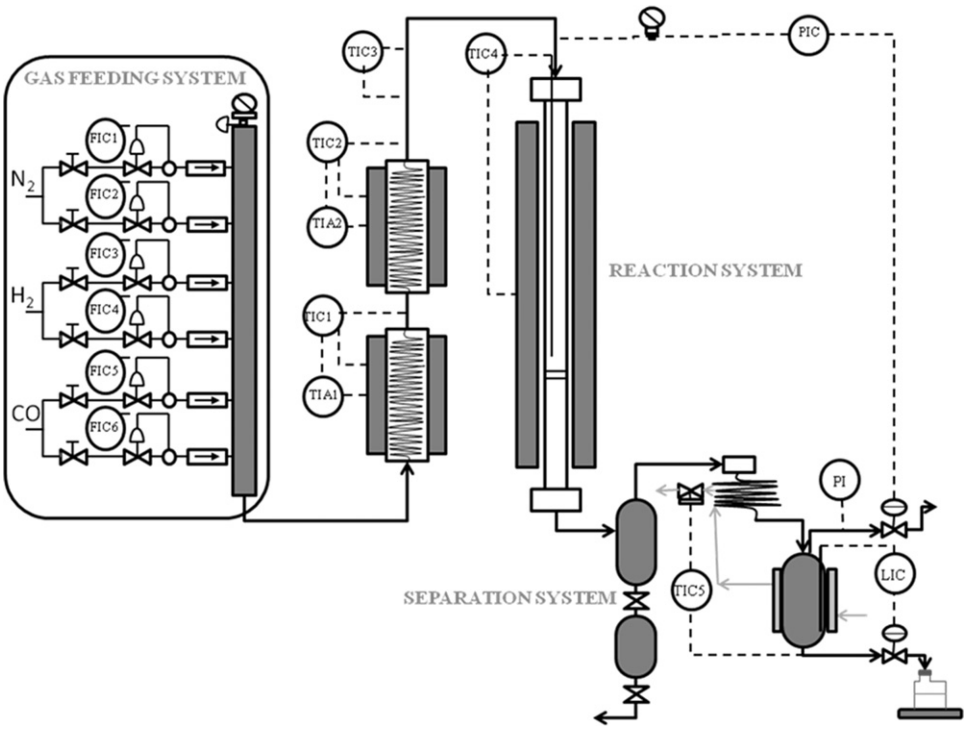

Fig. 1. Simplified process diagram of the bench scale set up for FTS.

alysts is scarce [17] and there are only some separately studies on the magnesium [18] or calcium [19] promoter effect. It is believed that the alkali addition to cobalt leads to an enhanced adsorption of carbon monoxide [20] and that the growth probability of Fischer–Tropsch synthesis increases up to $\alpha = 0.87$ in the presence of alkali promoter [21]. However there is not any study of comparison between alkali-earth and alkali metal promoter on FTS activity and selectivity over cobalt-based catalyst.

The aim of the present work was to study the effects of the addition of different alkali and alkali-earth oxides as promoters of a cobalt-alumina based catalyst on the FTS activity and product distribution, using a bench-scale experimental device.

2. Experimental

2.1. Bench scale set-up description

The facility which is fully automated and computerized consists of three physically separated parts: feed (gas and liquid) and mixing supply system, reaction system and products analysis system.

N_2, H_2 and CO (high purity supplied by PRAXAIR) are fed as the main gases. Each of these gases can be fed through two separate lines that have the same elements but different flow rates. The bench scale set-up included an Inconel fixed bed reactor (17.7 mm ID and 1000 mm length) for FT experiments.

The gaseous effluent was connected to the input of a gas chromatograph by means of a Peltier cell. The analysis system consisted of both gas analysis system and liquid analysis system. The first one consisted of a MicroGC (CP-4900 MicroGC VARIAN) with two analysis columns (Molsieve 5A for H_2, N_2, CH_4 and CO and Pora Pack Q column for CO_2, ethane and propane) using Ar and He as carrier gases, respectively. The liquid product distribution was measured using a GC-FID (Trace GC Ultra (Thermo Fisher Scientific)), which included an ultrafast capillary microcolumn.

Fig. 1 shows a schematic diagram of the experimental bench scale plant for FT reaction.

2.2. Catalyst preparation

2.2.1. Co/Al_2O_3

Catalyst Co/Al_2O_3 was prepared by incipient wetness impregnation. The support, γ-Al_2O_3, BET surface area 125 $m^2\,g^{-1}$ and pore volume 0.24 $cm^3\,g^{-1}$ was impregnated with an aqueous solution of cobalt nitrate [$Co(NO_3)_2{\cdot}6H_2O$] using two-steps incipient wetness to give a final catalyst with 20 wt% cobalt. After each impregnation, the catalyst was dried at 120 °C for 2 h. After the last impregnation and drying, the catalyst was calcined at 550 °C for 6 h.

2.2.2. $M\text{-}Co/Al_2O_3$

Alkali-modified alumina-supported cobalt catalysts were prepared by sequential impregnation. Alkali oxide-modified support was prepared by impregnating γ-Al_2O_3 with corresponding alkali nitrate aqueous solution. The sample was dried at 120 °C overnight and calcined in air at 550 °C for 6 h. Four samples with Ca, Mg, K and Na content of 1.0 wt% of metal promoter were prepared. Then, cobalt was impregnated into the alkali oxide-modified support to produce a catalyst with 20 wt% cobalt using the same procedure as in Section 2.2.1. The alkali-promoted catalysts were denoted as $M\text{-}Co/Al_2O_3$, where M refers to alkali or alkali-earth metal in the support. Table 1 shows alkali and cobalt content.

3. Catalyst characterization

3.1. Atomic absorption (AA)

In order to quantify the total amount of metal into the catalyst, atomic absorption (AA) measurement, with an error of ±1%, was made using a SPECTRAA 220FS analyzer with simple beam and background correction. The sample was previously dissolved in hydrofluoric acid and diluted to the interval of measurement.

Table 1
Chemical composition and physical properties of FTS catalysts.

Sample	wt% alkali	wt% Co	BET area ($m^2\,g^{-1}$)	D_{pore} (nm)	Total pore volume ($cm^3\,g^{-1}$)	Dispersion (%)[a] (H_2-ads.)	dCo^0 (nm)[b] (H_2-ads.)	dCo_3O_4 (nm)[c] (XRD)	dCo^0 (nm)[d] (XRD)	Metallic surface area (m^2/g_{metal})	HCl consumption ($pK_i \leq 7$) ($cm^3\,g^{-1}$)	Weak basicity ($mmol\,g^{-1}$)	Strong basicity ($mmol\,g^{-1}$)
Al_2O_3	–	–	125.4	7.5	0.236	–	–	–	–	–	–	0.092	0.010
Co/Al_2O_3	–	16	92.1	6.4	0.147	1.2	90.5	28.8	21.6	7.9	1.6	0.108	0.010
$Ca\text{-}Co/Al_2O_3$	0.6	17	84.3	6.8	0.144	2.0	52.8	55.6	41.7	13.8	2.8	0.130	0.053
$Mg\text{-}Co/Al_2O_3$	0.4	14	85.8	6.9	0.148	2.4	46.0	31.8	23.9	15.9	1.2	0.104	0.060
$K\text{-}Co/Al_2O_3$	0.4	16	76.3	7.0	0.134	2.2	46.6	76.6	57.5	15.1	3.2	0.182	0.062
$Na\text{-}Co/Al_2O_3$	0.6	14	96.5	6.3	0.152	1.9	54.8	40.0	30.0	13.2	2.4	0.138	0.041

[a] Co^0 dispersion from H_2 chemisorption at 308 K, assuming adsorption on Co atoms only.
[b] Co^0 particle size calculated from H_2 chemisorption using $d(Co) = 96/D$.
[c] Co_3O_4 particle size calculated from XRD of calcined catalyst using the most intense peak located at $2\theta = 36.9^\circ$.
[d] Co^0 particle size calculated from XRD using $d(Co) = 0.75 dCo_3O_4$.

3.2. Textural characteristics

Surface area/porosity measurements, with an error of ±3%, were conducted using a Micromeritics ASAP 2010 sorptometer apparatus with N_2 (at 77 K) as sorbate. Prior to analysis, the samples were outgassed at 433 K under vacuum (6.6×10^{-9} bar) for 16 h. The total specific surface areas were determined by the multi-point BET method and pore size distributions were evaluated using the standard BJH treatment [22].

3.3. X-ray powder diffraction (XRD)

X-ray diffraction patterns were determined by a Philips model X'Pert MPD with co-filtered Cu Kα radiation (λ = 1.54056 Å). The spectra were recorded from $2\theta = 3^\circ$ to 90° with 0.04° step using a 0.4 s acquisition time per step. The identification of the phases was made with the help of JCPDS files (joint committee on powder diffraction standards). The average crystallite size of Co_3O_4 was calculated according to Scherrer's equation [23].

3.4. Temperature programmed reduction (TPR)

TPR measurements of the catalysts were carried out in an Autochem HP 2950 analyzer. After loading, the sample was outgassed by heating at $10\,^\circ C\,min^{-1}$ in an argon flow up to the calcination temperature of the sample and kept constant at this temperature for 30 min. Next, it was cooled to room temperature and stabilized under an argon/hydrogen flow (≥99.9990% purity, 83/17 volumetric ratio). The temperature and detector signal were then continuously recorded while heating at $10\,^\circ C\,min^{-1}$ up to 900 °C. The liquid formed during the reduction process was retained by a cooling trap placed between the sample and the detector. TPR profiles were reproducible, standard deviations for the temperature of the peak maxima being ±2%.

3.5. Thermal analysis (TG/DTG)

Thermal analysis, the thermogravimetric (TG) and differential thermogravimetric (DTG) analysis, of alkaline-nitrates used was conducted using a TA INSTRUMENTS model SDT Q600 apparatus. TG and DTG curves were recorded in flowing nitrogen in the range from room temperature to 600 °C (heating rate $10\,^\circ C\,min^{-1}$). For analysis, 7 mg of a sample was loaded in a platinum crucible.

3.6. Acid/base titrations

Acid/base titrations were performed in a Metrohm 686 titrator with a Dosimat 665 automatic dosager. Sample (25 mg) was immersed in 50 cm^3 solution of 0.1 M NaCl, basified to pH ca. 10.3 with NaOH (0.1 M) with constant stirring under a N_2 atmosphere. A 0.1 M HCl solution was used as the titrant, added dropwise ($3\,cm^3\,h^{-1}$). The starting NaCl solution served as a blank [24–26].

3.7. Temperature programmed desorption (TPD)

The CO_2 temperature programmed desorption (CO_2-TPD) analysis was performed in the same system as used in TPR analysis. CO_2-TPD was used to obtain information on the basic sites of the catalytic samples. The temperature of desorption and the maximum desorbed CO_2 were illustrative of the strength and amount of basic sites, respectively. The sample was firstly reduced by heating at $5\,^\circ C\,min^{-1}$ under a flow of hydrogen/argon from room temperature to 550 °C, holding this temperature during 120 min. After cooling to 50 °C under flow of helium, CO_2 was fed at a rate of 30 ml min^{-1} for 30 min. Later, the sample was purged with helium for 1 h in order to eliminate physisorbed species. The temperature

was ramped at 10 °C min^{-1} from 50 to 900 °C. Then, CO_2-TPD data were acquired. The basic site density was obtained by the integration of area under the curve. The average relative error in the basicity determination was lower than 3% [27].

3.8. H_2 chemisorption

H_2 adsorption isotherms were measured at 35 °C in a standard volumetric quartz apparatus (Micromeritics ASAP 2010) capable of obtaining a vacuum of 10^{-5} T or better. The reactor was loaded with 0.7 g of catalyst. Before measurements, the catalysts were reduced in flowing hydrogen with temperature programming from ambient to 550 °C at a rate of 5 °C min^{-1}. This temperature was maintained for 2 h. After reduction, the samples were evacuated for 0.5 h at 550 °C before cooling to 35 °C, and the adsorption isotherm was measured between 50 and 500 mmHg. The amount of hydrogen chemisorbed was determined by extrapolating the linear part of the isotherm to zero pressure. It is assumed that promoters do not contribute to the amount of hydrogen chemisorbed when calculating the dispersion [28] and that the adsorption stoichiometry is H:Co = 1. Assuming spherical particles, the Co^0 particle size (dp) is related to the dispersion (D) through the following formula [29]:

$$dp = \frac{96}{D} \quad (1)$$

The average relative error in the dispersion determination was ±16%.

4. Activity test

Fischer–Tropsch synthesis was performed under 20 bars, which is an operating pressure representative of the pressurized gasification industrial process. A weighed sample of catalyst (5 g) was packed in the bench scale Inconel reactor between layers of inert material (SiC). Prior to Fischer–Tropsch synthesis, the catalyst was pretreated at atmospheric pressure by reduction with pure H_2 at 550 °C (heating rate 5 °C min^{-1}) for 2 h. After reduction, the catalyst was flushed with N_2 at 220 °C getting pressure rise up to 20 bars. Catalytic activity has been studied in the temperature range of 210–300 °C. Gas space velocity (SV) was set on 6000 h^{-1} and H_2/CO molar ratio was fixed to 2 (1.8 measured by GC analyzer) by adjusting feed gas flow rate to provide the desired value. Once operating conditions remained stable, both effluent gas compositions before and after reaction were analyzed online, at 1 h intervals, by a CP-4900 Varian MicroGC (gas chromatograph). Selectivity to C_5^+ was calculated using the following equation:

$$C_5^+ \ \text{selectivity}(\%) = 100 - CO_2 \ \text{selectivity}(\%) - C_1\text{–}C_4 \ \text{selectivity}(\%) \quad (2)$$

Moreover, liquid product recovered after 8–10 h at constant temperature was pretreated in order to separate organic phase from aqueous phase by diluting with n-hexane. Hence, liquid hydrocarbon products distribution from organic phase was analyzed by a GC-FID (Trace GC Ultra) from Thermo Fisher Scientific. Diesel fraction was considered in the C_{15}–C_{18} hydrocarbon range.

5. Results and discussion

5.1. X-ray diffraction and H_2-chemisorption

XRD patterns of the catalysts are presented in Fig. 2. Only crystalline Co_3O_4 phase and γ-Al_2O_3 are observed after calcination. Peaks at 20° and 38.1° {3 1 1} are ascribed to γ-alumina support [30,31] whereas peaks at 77–79° that corresponds to less than 3% could be related to $CoAl_2O_4$ (lattice plane of {5 3 3}) [32] or even

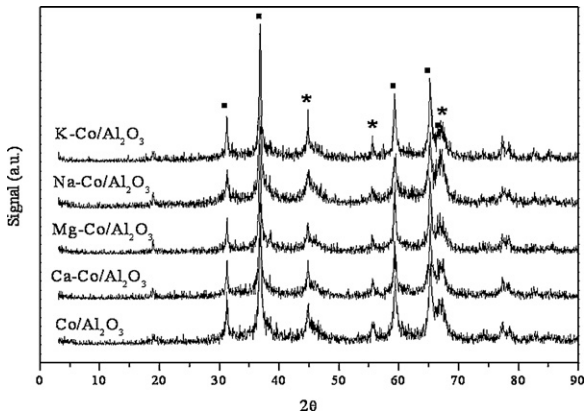

Fig. 2. XRD patterns for unpromoted and promoted-calcined Co/Al_2O_3 catalysts. ■: Co_3O_4; *: Al_2O_3.

from Al crucible. No peaks of Ca, Mg, K or Na-oxides are detected, indicating that alkali and alkali-earth oxides were dispersed on the support as a monolayer or formed spinel-like or tridymite-like structure with no detectable interaction between the promoter and support [33]. According to Bao et al. [19], alkali oxides promoted catalysts have a tendency to form larger Co_3O_4 particle than alkali oxide-free catalyst. It was noted that the average diameter was larger than the support pore diameter so that some large Co_3O_4 were located on the external surface of the support. The average Co_3O_4 particle size calculated for all catalysts from the Scherrer equation (2θ: 37° diffraction peak), together with the average Co^0 particle sizes obtained from H_2 chemisorption measurements, are presented in Table 1. From XRD patterns it can be seen an increase in cobalt crystalline size with alkali oxide promotion. As a consequence of these results, the reducibility of alumina supported cobalt promoted catalysts may be favored. The average Co_3O_4 particle size, as determined by XRD, was the smallest for the Co/Al_2O_3-supported catalyst. The largest Co_3O_4 particles were observed on the K-Co/Al_2O_3 catalyst.

H_2-chemisorption experiments showed very similar dispersion values for all promoted catalysts which were two times higher than the unpromoted one. Hence, similar average Co^0 particle size for promoted catalysts was found from the H_2 chemisorption results. In this case, the presence of a certain amount of alkali/alkali-earth promoter resulted in a decrease in the average Co^0 particle size. Differences in particle size from XRD and H_2 chemisorption may be due to cobalt phases interacting with the support, especially in case of unpromoted catalyst. If this phase is nonreducible at standard reduction condition, then it does not contribute to the particle size obtained from H_2 chemisorption and therefore a higher particle size was obtained for the unpromoted catalyst [34]. Thus, from Table 1 it can be concluded that the presence of a certain amount of alkali/alkali-earth promoter resulted in an enhancement of metallic active sites arising from the increased dispersion.

5.2. Nitrogen adsorption measurement

The summarized results of surface area and pore volume for both the support and the catalysts, calculated from the nitrogen adsorption–desorption isotherms, are provided in Table 1. Fig. 3a and b exhibits adsorption/desorption isotherms and BJH pore size distribution, respectively. The N_2 adsorption/desorption isotherm associated to all of these catalysts (Fig. 3a) can be accounted for as a type IV reference isotherms, according to the IUPAC classification. The hysteresis loop due to capillary condensation at higher partial pressures matches that observed for a type IV isotherm and is associated with mesoporosity [35]. Upon impregnation of

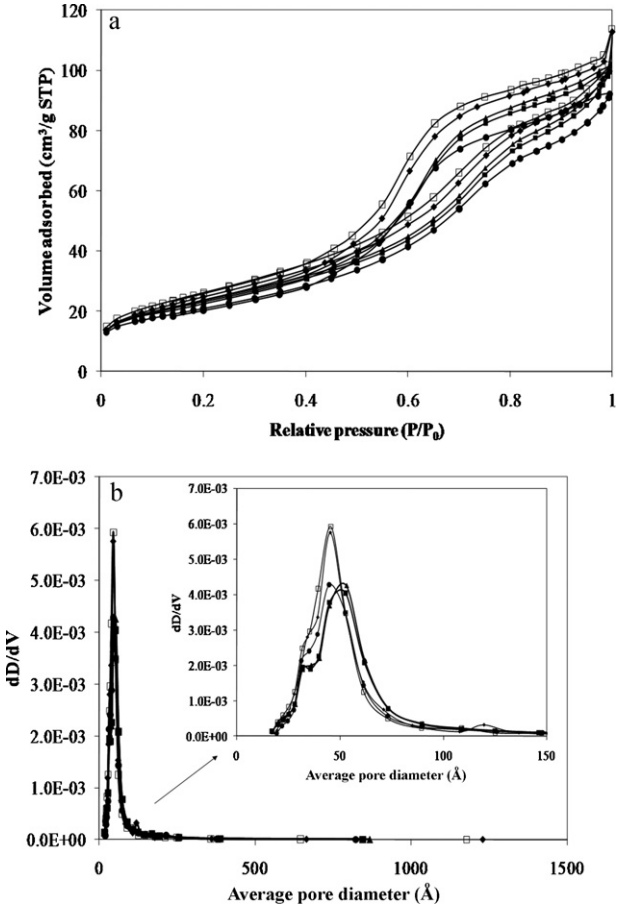

Fig. 3. (a) Adsorption/desorption isotherms. (b) Average pore diameter distribution. ●, Co/Al_2O_3; ■, $Ca\text{-}Co/Al_2O_3$; ▲, $Mg\text{-}Co/Al_2O_3$; □, $Na\text{-}Co/Al_2O_3$; ●, $K\text{-}Co/Al_2O_3$.

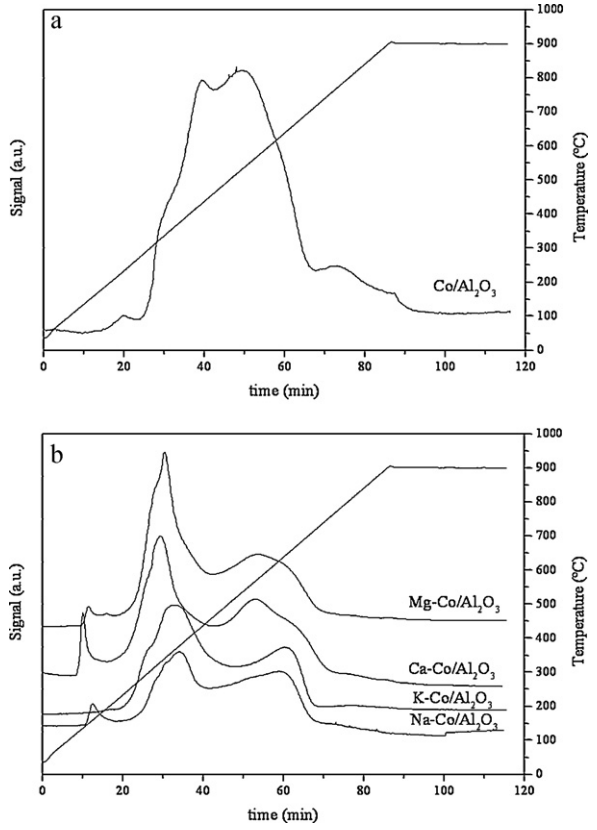

Fig. 4. TPR profiles: (a) unpromoted Co/Al_2O_3 catalyst and (b) promoted, calcined Co/Al_2O_3 catalysts.

both cobalt and alkali/alkali-earth-cobalt on the support, the surface area decreased, especially on promoted catalyst, indicating a partial blockage of pores by the metal species. The corresponding pore sizes shown in Table 1 are within the range of those that corresponds to mesopores (2–50 nm) [35]. The pore size distribution (Fig. 3b) exhibited a peak maximum ca. 4.2 nm and 4.5 nm in the case of alkali metal promoted catalysts and unpromoted catalyst, respectively, whereas alkali-earth promoted catalysts shifted to 5.3 nm. Due to uniform pore distribution of cobalt impregnated on Al_2O_3 support, the catalysts showed reduced pore volume and average size which means efficient deposition of cobalt species in the inner pore of Al_2O_3 support. It was also noted that average Co_3O_4 particle size measured by XRD was larger than the support pore size on all unpromoted and promoted catalysts. This may be considered mainly due to the deposition of a large fraction of the particles rather on the outside or occupying adjacent, interconnecting, pore cavities of Al_2O_3 support. Since cobalt–support interactions depend on the type of support and cobalt particle size, then, it can be expected that larger particle size result in weaker metal–support interaction, leading to high degree of the reduction of cobalt species.

5.3. H_2-temperature programmed reduction and TG/DTG

It is generally accepted that the active sites for Fischer–Tropsch synthesis over cobalt-based catalysts are reduced Co metal surface sites. As reported by Jacobs and coworkers, in the loading range of 15–25% Co, Co/alumina catalysts generally exhibit two peaks in TPR, a sharp peak close to 350 °C that corresponds to the reduction of Co_3O_4 to CoO, and a very broad peak at higher temperature that corresponds to the reduction of CoO to metallic Co and is heavily dependent on support type, porosity and crystallite size [36]. Thus, the presence of a peak that extends up to temperatures as high as 800 °C can be ascribed to species of cobalt-aluminates. TPR profiles of the catalysts are displayed in Fig. 4a and b, respectively.

As depicted in Fig. 4a, two major peaks for catalyst Co/Al_2O_3 were observed at temperature ranges of 420–455 °C, respectively. The first peak could be assigned to the reduction of Co_3O_4 to CoO. Jacobs et al. [36] also showed that Co_3O_4 underwent virtually 100% transition to CoO prior to the formation of Co below 400 °C. The second peak was ascribed to the subsequent reduction of CoO to Co^0 however, the existence of cobalt aluminate species could not be excluded as was evidenced by the peak observed at 760 °C. Besides these reduction peaks, a small peak appeared at about 225 °C. Some authors attributed this peak to the reduction of residual cobalt nitrate [9,23,37], which decomposed completely above 400 °C. In order to clarify the assignment of this peak a TG/DTG analysis was done. Fig. 5 shows that the decomposition of $Co(NO_3)_2{\cdot}6H_2O$ in nitrogen was found to occur in four consecutive endothermic processes. The latter one at 275 °C was ascribed to the total transformation of cobalt nitrate to Co_3O_4 [38]. Since calcination temperature was set on 550 °C, and according to DTG results, the reduction peak at 225 °C was not attributed to the reduction of residual cobalt nitrate but to an incipient beginning of the reduction of Co_3O_4 to CoO, as previously reported by Khodakov et al. [39].

Fig. 4b illustrates TPR profiles of metal promoted catalysts. Alkali-earth promoted catalysts showed a similar TPR trend. Catalyst $Ca\text{-}Co/Al_2O_3$ presented two main peaks at 337 °C and 570 °C and catalyst $Mg\text{-}Co/Al_2O_3$ exhibited two main peaks at 342 °C and 577 °C, respectively. Besides these two reduction peaks, it also appeared that the first peak attributed to incipient beginning of

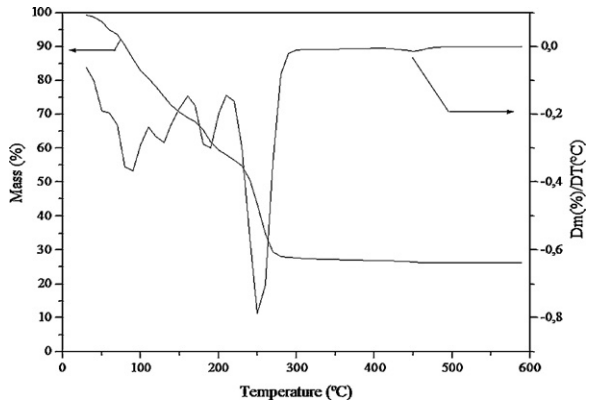

Fig. 5. TG/DTG curves of Co-nitrate.

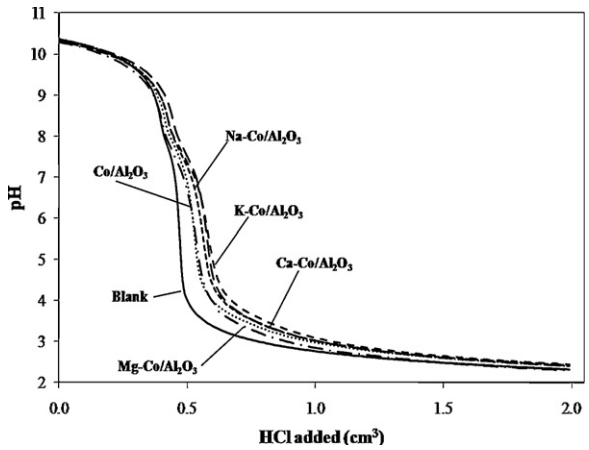

Fig. 6. Acid/base titration curves associated with blank, Co/Al_2O_3 and promoted Co/Al_2O_3 catalysts.

the reduction of Co_3O_4 to CoO [40,41] shifted about 80 °C (Ca-Co/Al_2O_3) and 73 °C (Mg-Co/Al_2O_3) to lower temperature than for the unpromoted catalyst. TG and DTG analysis of alkali-earth nitrate salts (not shown) demonstrated that decomposed at temperatures lower than 500 °C. The relative contribution of the species reduced at lower temperatures can be ascribed to the lower strength of interaction between Co^{2+} and alumina support. TPR data revealed that the addition of alkali-earth metal promoters caused changes in reduction behavior of the Co catalysts. As a consequence, the peak associated with cobalt-aluminate compounds was not present in these profiles.

Alkali metal promoted catalysts also showed a similar reduction behavior than alkali-earth metal promoted catalysts. Catalyst Na-Co/Al_2O_3 presented two main peaks at 374 °C and 633 °C, while catalyst K-Co/Al_2O_3 shifted to 368 °C and 647 °C, respectively. Besides these two reduction peaks, a small first peak also appeared at about 160 °C in case of catalyst Na-Co/Al_2O_3. This peak was negligible for K-Co/Al_2O_3 TPR profile. TG and DTG analysis of Na-nitrate (not shown) indicated that thermal decomposition still continued at temperatures higher than 500 °C. Then, TPR peak at 160 °C could be ascribed to either thermal decomposition or reduction of residual nitrate [42]. The peak associated with cobalt-aluminate compounds was neither present in these profiles. As shown with alkali-earth-promoted catalysts, alkali-promoted catalysts were noted to facilitate the reduction step. However, as alkali-metal promoted catalyst possessed greater basicity according to CO_2-TPD analysis (Table 1), the H_2 adsorption can be diminished and led to a decrease in the H_2 concentration on the catalyst surface; therefore, the reducibility of these catalysts declined at higher temperatures [15].

From TPR and H_2-chemisorption results, it can be concluded that the presence of a certain amount of alkali/alkali-earth promoter seemed to favor reducibility if compare with the unpromoted catalyst. Moreover, the greater activity of promoted catalysts with respect to the unpromoted one could be justified by the enhancement of metal dispersion.

5.4. Acid–base titrations and CO_2-temperature programmed desorption

Fig. 6 presents the acid/base titration curves related to each of the catalysts studied. The curves were displaced to higher HCl consumption values in the following order: Mg-$Co/Al_2O_3 \sim Co/Al_2O_3 <$ Ca-$Co/Al_2O_3 \sim$ Na-$Co/Al_2O_3 <$ K-Co/Al_2O_3, which was consistent with the oxides structure and their position in periodic table. Surface basicity values, expressed as cm^3 HCl consumed per gram of catalyst to achieve $pH \leq 7$, are recorded in Table 1. These measurements essentially represent the total number of surface basic sites and confirmed the introduction of surface basicity post-alkali promotion. As expected, alkali promoted catalysts, especially K-Co/Al_2O_3, showed higher basicity values than alkali-earth promoted catalysts.

Fig. 7 illustrates the CO_2-TPD profiles for these samples. Alkali promoted samples showed a single desorption peak at approximately 150 °C which can be attributed to the interaction of CO_2 with sites of weak basic strength. Alkali-earth promoted samples exhibited a broad desorption peak with two maxima at approximately 105 °C and 150 °C which also can be related

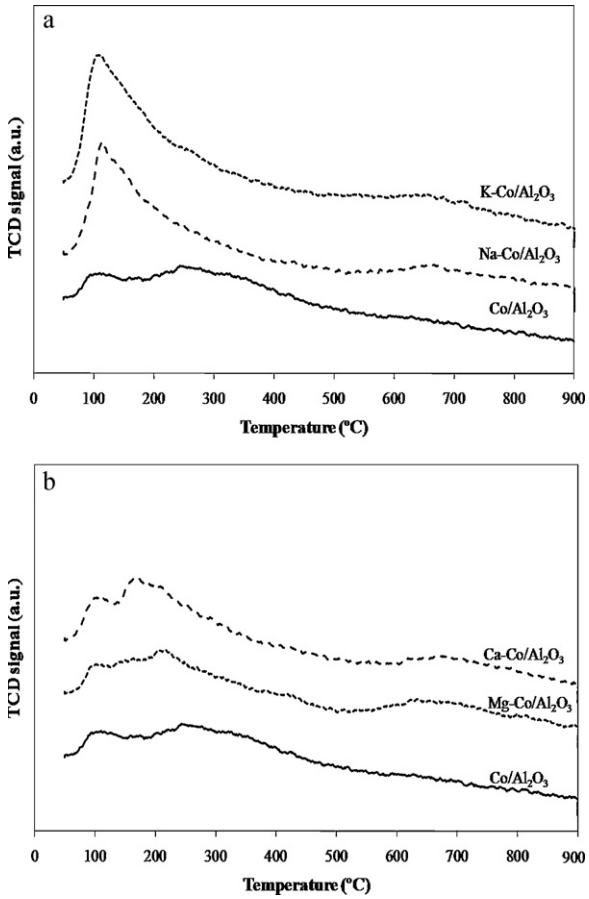

Fig. 7. CO_2-TPD profiles: (a) alkali promoted catalysts and (b) alkali-earth promoted catalysts.

to the desorption of physically adsorbed CO_2 in the metallic phase. The amount of desorbed CO_2 resulting from the addition of alkali or alkali-earth metal promoters were larger than that observed for the sample Co-Al_2O_3 as recorded in Table 1. Catalyst basicity increased in the order: Mg-Co/Al_2O_3 ~ Co/Al_2O_3 < Ca-Co/Al_2O_3 < Na-Co/Al_2O_3 < K-Co/Al_2O_3, confirming the results obtained by acid–base titration technique. In all the samples, a small second desorption peak appeared at higher temperatures (650–675 °C), which may be ascribed to the decomposition of a small amount of metal carbonates formed during CO_2 adsorption [43].

The crystalline structure of the Al_2O_3 support was not altered, as confirmed by XRD analysis. However, the BET surface areas and total pore volumes exhibited a decrease in all the cases, especially K-Co/Al_2O_3. This behavior has been previously reported and attributed to a partial pore blockage. It was difficult to link differences in surface areas to catalyst basic behavior. Accordingly, some studies provided evidence that it was not only the amount of promoter which was important but also the surface area of the catalyst as well as the chemical nature of the other additives or impurities present. Thus, the intrinsic basicity of the alkali promoter must be above certain strength and the promoter must also cover a certain fraction of the catalyst surface [44]. It should be also noted that basicity values greatly correlated to particle size measured by XRD confirming that the addition of alkali and alkali-earth promoter have a tendency to form larger Co_3O_4 particle than alkali-free catalyst, as commented before. However, it has been observed from H_2-chemisorption results that the presence of alkali and alkali-earth promoters favored metallic active sites. Thus, the greater activity of promoted catalysts with respect to the unpromoted one could be justified by the enhancement of metal dispersion whereas the basic behavior could influence C_5^+ hydrocarbon product distribution.

5.5. Fischer–Tropsch synthesis

The current focus on the FTS process deals with the production of transportation fuel such us diesel, which can be maximized via oligomerization or hydrocracking of FTS effective hydrocarbons. Therefore, it is expected that more effective hydrocarbons are produced via selectivity control, the addition of promoters or some other feasible ways. It have been also demonstrated that the addition of a strongly basic alkaline promoter is required to shift the selectivity toward the more useful long-chain hydrocarbons [44]. It is well known that the addition of alkali to iron catalyst causes and increase in both 1-alkene selectivity and the average carbon number of produced hydrocarbons [45,46]. Studies on the promoter effect of alkali on cobalt are rare due to the decrease in the FTS rate by the alkali addition. However, recent studies have shown that some alkali oxide promoters involve larger Co_3O_4 particles resulting in high reducibility that provides more cobalt active sites and hence, increased the catalytic activity. On the other hand, cobalt aluminate species hardly to reduce should be avoided [19,22,47–49].

5.5.1. CO conversion

The steady-state performance of each cobalt-based catalyst at 20 bars and temperatures between 210 °C and 300 °C, after 6–7 h, is illustrated in Fig. 8 and characterized in Table 2. For a synthesis gas of $H_2/CO = 2/1$, data results of CO conversion over the catalysts promoted with Na and K from Group I alkali metals, Ca and Mg from Group II-alkali-earth metals and unpromoted catalyst were recorded. CO conversion seemed to be deeply dependent on increasing reaction temperature. As expected, CO conversion was enhanced, C_1–C_4 fraction was increased and C_5^+ fraction diminished by increasing reaction temperature in all the samples. As

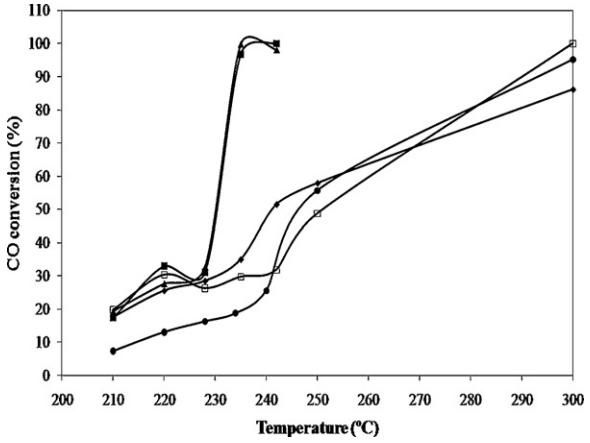

Fig. 8. Influence of temperature on CO conversion for alkali-promoted and non-promoted catalysts. ◆, Co/Al_2O_3; ■, Ca-Co/Al_2O_3; ▲, Mg-Co/Al_2O_3; □, Na-Co/Al_2O_3; ●, K-Co/Al_2O_3.

reported by Farias et al. and Tian et al. it was found that the increasing temperature promotes CO dissociation and provides more surface C atoms for forming hydrocarbons. On the other hand, the abundant surface H leads to more methane formation with increasing reaction temperature [50,51].

In order to study the effect on Fischer–Tropsch synthesis activity and selectivity clearly, 220 °C, 242 °C and 300 °C were chosen as representative temperatures of lower CO conversion and higher CO conversion values for alkali-earth and alkali metal promoted catalysts, respectively. It is important to note that alkali-metal promoted catalysts presented a different behavior to alkali-earth-metal promoted catalysts.

At lower CO conversion values (220 °C), unpromoted catalyst showed slightly lower activity to that of alkali-earth catalysts and sodium-promoted catalysts but potassium-promoted catalyst yielded the lower CO conversion (up to approximately 250 °C). In agreement with these results, it was found that the addition of small amounts of potassium (0.0016–0.0066%) used as promoter of cobalt/CNTs supported catalysts resulted in decreasing FTS rate. It was also reported that the addition of 1.65–4% of K to Mn-Ru/alumina decreased the activity of the catalyst for total hydrocarbons production needing higher temperatures than 240 °C to reach similar FTS conversion values. Thus, potassium promotion is found to may block (simply physically cover) the low-coordination edge and corner sites for dissociative adsorption of hydrogen so that the mobility of hydrogen is significantly restricted [52–54] declining catalytic activity.

It can be noted that there seemed to be a direct relationship between Co particle size of promoted catalysts and CO conversion with the exception of potassium promoter. As some authors have reported [19], the higher the particle size the higher the reducibility and, as a consequence, the higher catalytic activity. Co particle size was related to basic behavior of catalyst. Thus, these results suggested a direct proportionality between surface basicity and hydrogenation rate [55]. Moreover, hydrogenation rate must be favored by increasing metal active sites (as reported in Table 1) which is related to the metallic dispersion. Hence, both effects were observed to influence CO conversion.

At 242 °C, alkali-earth promoted catalysts deeply raised CO conversion to the highest value (96–100%). Na- and K-promoted catalyst slightly increased their conversion up to 25–31%, respectively, being 300 °C needed to reach their higher CO conversion value. These results are in agreement with those reported by Luo et al. [56] that needed 270 °C to increase CO conversion to 50%. Unpromoted catalyst followed a similar trend to alkali metal

Table 2
Influence of temperature. GHSV: 6000 h^{-1}. H_2/CO: 2.

Catalyst	T (°C)	Co rate (mol/mol Co h)	FTS rate (mol/mol Co h)	CO_2 rate (mol/molCo.h)	X_{CO} (%)	X_{H_2} (%)	Hydrocarbon selectivity (%)				
							CO_2	C_1–C_4	O/O + P (C_2)	O/O + P (C_3)	C_5^+
Co/Al_2O_3	210	5.1	5.08	0.01	17.6	31.6	0.18	1.77	0.75	1.00	98.05
	220	7.4	7.37	0.02	25.6	39.6	0.22	4.28	0.62	1.00	95.50
	228	11.2	11.18	0.02	28.8	55.9	0.23	3.13	0.27	0.93	96.64
	235	10.6	10.56	0.06	32.1	42.5	0.60	7.76	0.16	0.92	91.64
	242	14.9	14.80	0.07	51.5	53.4	0.48	5.61	0.14	0.92	93.91
	250	16.7	16.61	0.11	57.9	72.6	0.67	5.94	0.09	0.87	93.39
	300	24.9	24.32	0.57	86.2	92.2	2.29	10.27	0.07	0.82	87.44
Ca-Co/Al_2O_3	210	4.8	4.79	0.01	17.3	24.7	0.25	2.13	0.66	1.00	97.62
	220	9.2	9.15	0.01	33.0	46.2	0.18	4.39	0.69	1.00	95.43
	228	8.6	8.60	0.03	31.1	43.1	0.31	3.35	0.53	0.98	96.34
	235	27.6	22.96	3.92	96.7	93.4	14.59	44.34	0.01	0.46	41.07
	242	27.8	23.59	4.20	100.0	97.4	15.10	45.53	0.00	0.00	39.37
Mg-Co/Al_2O_3	210	6.4	6.46	0.02	19.2	29.0	0.23	2.95	0.61	1.00	96.82
	220	9.3	9.27	0.02	27.5	34.9	0.23	5.48	0.65	1.00	94.29
	228	11.0	10.92	0.05	32.5	41.5	0.45	5.49	0.37	0.98	94.06
	235	33.7	28.60	5.06	99.8	97.2	15.03	46.12	0.00	0.98	38.85
	242	33.1	27.58	5.52	98.1	93.5	16.69	53.10	0.00	0.53	30.22
K-Co/Al_2O_3	210	2.2	2.14	0.01	7.3	10.7	0.59	6.26	0.67	1.00	93.14
	220	3.8	3.82	0.02	13.0	16.4	0.54	10.25	0.69	1.00	89.21
	228	4.8	4.64	0.15	16.2	22.0	3.08	10.25	0.40	1.00	82.44
	235	5.8	5.53	0.24	18.7	24.6	4.21	15.02	0.30	0.98	80.77
	242	7.6	7.55	0.10	25.6	37.0	1.49	12.62	0.30	0.98	85.90
	250	16.4	15.10	1.32	55.6	66.3	8.06	23.93	0.07	0.88	68.01
	300	28.1	23.74	4.36	95.2	90.9	15.51	33.18	0.01	0.30	51.31
Na-Co/Al_2O_3	210	6.9	6.93	0.01	19.7	33.9	0.16	0.85	0.81	1.00	99.0
	220	10.7	10.67	0.02	30.3	47.4	0.17	1.82	0.76	1.00	98.0
	228	9.3	9.24	0.03	26.3	43.3	0.27	1.85	0.69	1.00	97.9
	235	10.5	10.44	0.04	29.7	45.4	0.38	2.81	0.53	0.98	96.8
	242	11.3	11.17	0.07	31.9	45.0	0.65	4.80	0.42	0.96	94.6
	250	17.2	17.06	0.11	48.7	56.9	0.64	1.97	0.33	0.95	97.4
	300	35.3	30.04	5.21	100.0	94.2	14.79	35.83	0.01	0.62	49.4

promoted catalysts. An explanation for alkali-earth promoted catalysts behavior at 242 °C could be found in terms of hydrogen spillover. On this basis, the enhanced CO and H_2 conversions and the increased CH_4 selectivity (Table 2 and Fig. 10) can be well explained [57].

From these data, it can be concluded that the CO conversion improved in the presence of alkali/alkali-earth promoter due to an enhancement of dispersion with consequently increase in active sites at the same time reducibility is favored, with the exception of K-Co/Al_2O_3.

5.5.2. Hydrocarbon selectivity

It is well known that the CO conversion level has an important impact on relative activities of FTS and WGS reaction over cobalt-based catalyst, resulting in different product selectivity values. The WGS reaction is a side-reaction accompanied with FTS. The CO can be converted to either hydrocarbon by FTS reaction or CO_2 via WGS reaction. Then, the rate of CO_2 formation is equal to the rate of the WGS.

Figs. 9–12 show the selectivity to carbon dioxide, C_1–C_4 fraction and higher hydrocarbons (C_5^+) fraction obtained by FTS reactions catalyzed with both alkali-earth and alkali-metal promoted catalysts and unpromoted catalyst, respectively. Methane selectivity and lightweight hydrocarbons (C_1–C_4) showed an opposite trend to C_5^+ selectivity.

From these figures and data depicted in Table 2, it can be observed that, at lower conversion levels (220 °C), FTS is relatively rapid compared to WGS so that a higher fraction of CO was converted to hydrocarbons. The addition of alkali-earth and alkali metal promoters (except for K) seemed to favor FTS rate suggesting inhibition of WGS reaction [16]. At this lower selectivity to CO_2, potassium promoter showed the highest selectivity value. This fact may be attributed to the tendency of larger cobalt particles for H_2O adsorption, which presumably participate in WGS reaction, and leads to the production of CO_2 [58,59].

The advantage of the more rapid FTS rate cannot be maintained through CO conversion since the decreasing H_2/CO ratio causes the rate determining step to change from FTS to the WGS reaction. Thus, at 242 °C, WGS rate and, consequently, selectivity to CO_2 increased, especially for alkali-earth metal promoted catalysts, while 300 °C was needed in case of alkali metal promoted catalysts (Fig. 9). Accordingly to these results, selectivity to C_1–C_4 fraction was strongly increased at 242 °C for Ca- and Mg-promoted catalysts (from 5% to 45–50%) and at 300 °C for Na- and K-promoted catalysts (up to 35%), respectively. As a consequence, selectivity to C_5^+ diminished up to 30% using alkali-earth catalyst while a 50% was maintained in case of alkali metal catalyst.

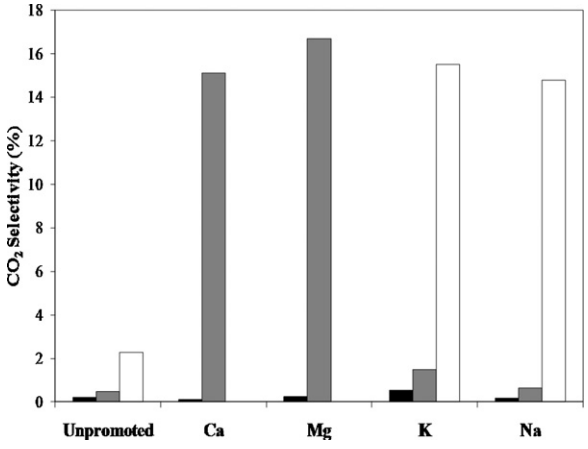

Fig. 9. Influence of temperature on selectivity to CO_2 for alkali-promoted and non-promoted catalyst. ■: 220 °C, ▩: 242 °C, and □: 300 °C.

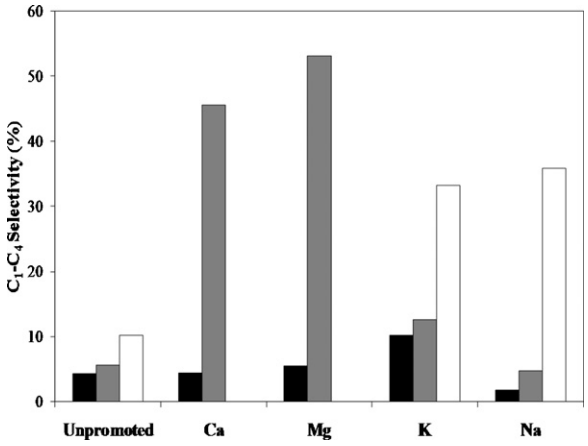

Fig. 10. Influence of temperature on selectivity to C_1–C_4 for alkali-promoted and non-promoted catalysts. ■: 220 °C, ▩ : 242 °C, and □: 300 °C.

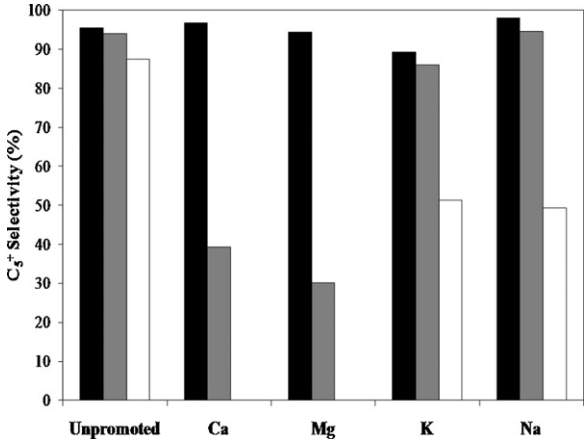

Fig. 11. Influence of temperature on selectivity to C_5^+ for alkali-promoted and non-promoted catalysts. ■: 220 °C, ▩ : 242 °C, and □: 300 °C.

Usually, high methane selectivity has been reported for low reducibility and high dispersion [60] attributed to the presence of unreduced cobalt oxides catalyzing the WGS reaction, thus increasing the effective H_2/CO ratio at the catalyst surface. Ca oxide used as promoter of cobalt-based catalyst have been reported [19] to favor CO conversion and selectivity to C_5^+ and as shown in TPR profiles (Fig. 4b) alkali-earth promoted catalysts were found to enhance

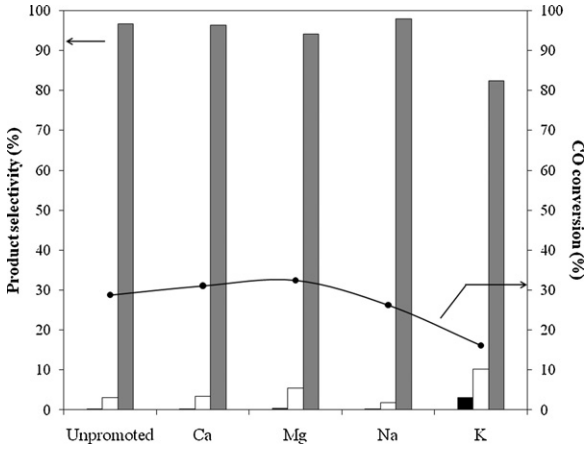

Fig. 12. Influence of promoters on product selectivity. Reaction temperature: 210 °C. Selectivity: ■: CO_2, ▩ : C_1–C_4, and □: C_5^+; ●— CO conversion.

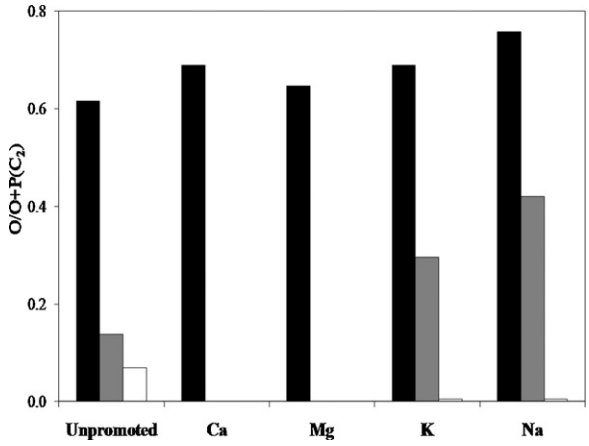

Fig. 13. Influence of temperature on O/O + P (C_2) for alkali-promoted and non-promoted catalysts. ■: 220 °C, ▩ : 242 °C, and □: 300 °C.

reducibility. However, our results showed a strong increase in CO_2 and C_1–C_4 fraction and reduced the formation of C_5^+. The increase in the CO_2 formation rate can be attributed to the increase in water partial pressure due an increase in FTS reaction rate [61]. The excessive methane formation can be attributed to hydrogen spillover related to a strong increase in CO conversion and H_2 conversion, as commented before.

Accordingly with Trépanier et al. [52], alkali metal promoted catalysts produced lower methane selectivity. This fact can be explained on the basis of partial pressure of hydrogen atoms on alkalinized catalyst surface which in turn leads to a decrease in the rate of chain termination step to paraffins (i.e. methane) in the course of FT reaction. Increase in selectivity of higher molecular weight hydrocarbons can be explained by the increased concentration of α-olefins and readsorption and chain initiation of these primary products on catalyst surface which lead to the ultimate desorption of these α-olefins as larger products [62].

Finally and in order to make proper comparisons between catalysts Fig. 12 shows product selectivity obtained by the different catalysts at a fixed temperature of 210 °C and similar CO conversion. Similar trend was observed at 228 °C. The only exception was K-promoted sample that kept conversion under the desired value until 250 °C. Hence, similar product distributions were observed for unpromoted, Ca and Na promoted catalysts and a decrease in C_5^+ formation in favor of CH_4 production for Mg-promoted sample and especially for K-promoted one.

Olefin ratio (O/O + P) was calculated from the following equation:

$$\text{olefin ratio} = \frac{\text{olefin}}{\text{olefin} + \text{paraffin}} \quad (3)$$

Figs. 13 and 14 show the olefin ratio from FTS over unpromoted catalyst and alkali-metal and alkali-earth metal promoted catalysts. The data showed that all unpromoted, alkali-metal and alkali-earth metal promoted catalysts yielded similar C_3 olefin ratio at 220 °C. The ethylene fraction, presented a slightly decrease from Na-promoted catalyst to unpromoted catalyst, although similar trend was observed for all the samples. At 242 °C, a propylene fraction of 0.96–0.98 was obtained for alkali metal catalysts, which was slightly higher than that of unpromoted catalyst (0.92). However, Mg-promoted catalyst reduced this fraction to 0.53 while it was negligible in case of Ca-promoted catalyst. A similar effect was observed for ethylene fraction. Na- and K-promoted catalyst resulted in 0.42 and 0.30 values, respectively higher than that of 0.14 of the unpromoted catalyst. Ca- and Mg-promoted catalysts did not produce ethylene. These results are in agreement with those reported by Luo and Davis [63] and Gaube and Klein [17] where

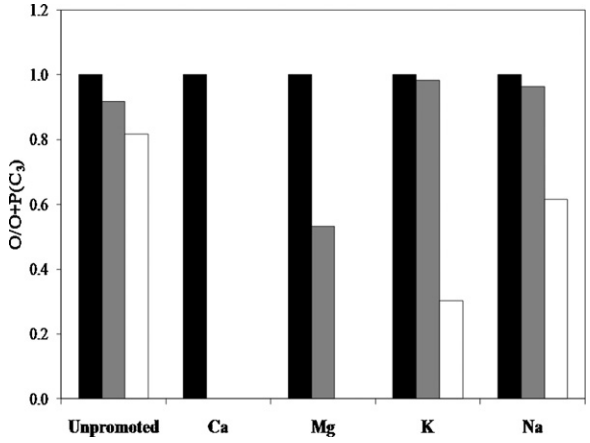

Fig. 14. Influence of temperature on O/O+P (C_3) for alkali-promoted and non-promoted catalysts. ■: 220 °C, ▩ : 242 °C, and □: 300 °C.

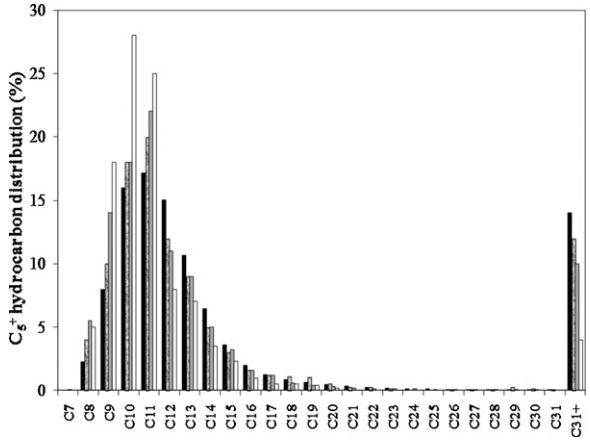

Fig. 15. Influence of temperature on C_5^+ hydrocarbon distribution. Co/Al_2O_3 catalyst. ■: 220 °C, ▩ : 235 °C, ▩ : 242 °C, and □: 300 °C.

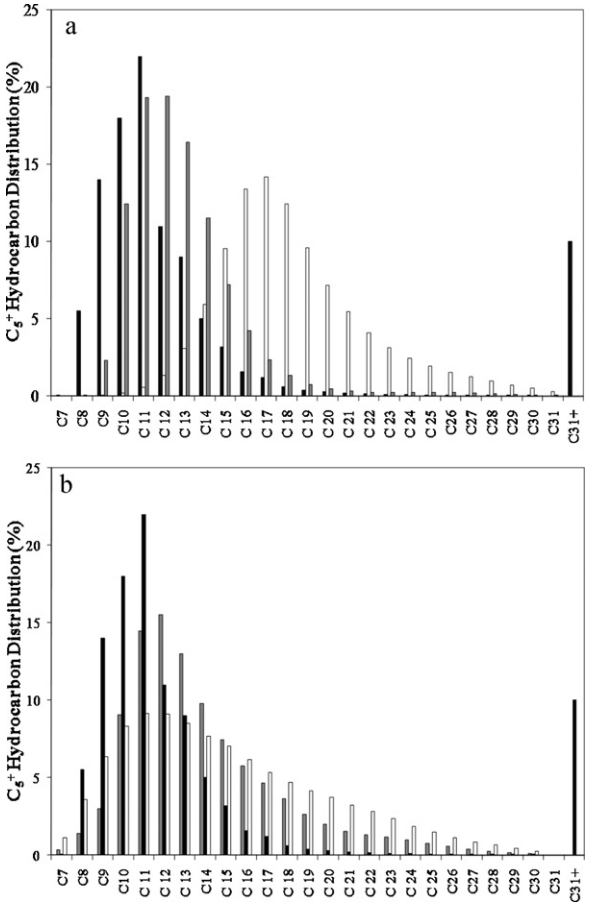

Fig. 16. (a) Influence of alkali-earth promoters on C_5^+ hydrocarbon distribution. ■: Co/Al_2O_3, ▩ : Mg-Co/Al_2O_3, □: Ca-Co/Al_2O_3; (b) influence of alkali promoters on C_5^+ hydrocarbon distribution. ■: Co/Al_2O_3, ▩ : Na-Co/Al_2O_3, and □: K-Co/Al_2O_3. Reaction temperature: 242 °C.

the addition of alkali metal causes an increase in 1-alkene selectivity. Thus, the addition of alkali metal promoter was suggested to suppress the hydrogenation activity better than alkali-earth metal promoters.

Finally and accordingly to Ngantsoue et al. [64], the fraction of alkenes was studied to decrease as the CO conversion increased.

Fig. 15 displays hydrocarbon distribution obtained with catalyst Co/Al_2O_3 at different temperatures. A similar behavior with temperature was observed for promoted catalyst. As expected, an increase in reaction temperature favors the shifting toward lighter hydrocarbons formation. However, at all temperatures studied, and especially at 220 °C, catalyst Co/Al_2O_3 yielded heavy paraffins, as a result of secondary reactions involving re-adsorption and incorporation of olefins into growing chains.

Fig. 16 and Table 3 show C_5^+ hydrocarbon product distribution for alkali and alkali-earth promoted catalyst and the non-promoted one. It was important to note that the promoter addition increases the production of higher molecular weight hydrocarbons without yielding heavy paraffins as compared with the free promoter cobalt-based catalyst. The increase on the cobalt particle size due to an increase on the basicity could be the responsible of this result, as discussed before. Mg and Ca promoted samples were found to favor higher molecular weight hydrocarbons but Ca sample shifted to mainly diesel production (49.7%) (Fig. 16a). Na and K promoted catalyst also shifted to higher molecular weight hydrocarbon product as can be observed in Fig. 16b. Both samples were found to raise similar diesel production (21.5% and 26%, respectively) but lower than Ca promoted catalyst despite the metallic particle size. Moreover K promoted sample showed higher waxes production than Na promoted one but very similar to Ca-promoted catalyst.

Taking into account the FTS results it can be concluded that the addition of Ca to the cobalt based catalyst greatly improved diesel selectivity. However Ca promoted catalyst yield a higher amount of methane at 242 °C than the Na sample.

Table 3
C_5^+ hydrocarbon product distribution.

Sample	Gasoline (C_7–C_{10}) (%)	Kerosine (C_{11}–C_{14}) (%)	Diesel (C_{15}–C_{18}) (%)	Lubricants (C_{19}–C_{20}) (%)	Waxes (C_{20}^+) (%)	Total diesel selectivity
Co/Al_2O_3	37.5	47.0	6.6	0.7	10.8	6.2
Ca-Co/Al_2O_3	0.3	10.9	49.7	16.8	22.4	19.5
Mg-Co/Al_2O_3	14.8	66.8	15.2	1.2	2.1	4.6
K-Co/Al_2O_3	11.1	35.1	26.2	8.8	18.8	22.5
Na-Co/Al_2O_3	13.8	52.8	21.5	4.6	7.2	20.4

6. Conclusion

A series of unpromoted and alkali and alkali-earth metal promoted cobalt/alumina based catalysts were prepared in order to study the effect of alkali oxide on the Fischer–Tropsch synthesis activity and selectivity in a single bench scale fixed bed reactor. XRD patterns, H_2-chemisorption and TPR results showed that both alkali and alkali-earth oxides suppress the interaction between cobalt oxide and support resulting in an increased cobalt reducibility and more cobalt active sites. A positive correlation between basicity and particle size was observed with the exception of K promoted sample. Furthermore, CO conversion and C_5^+ selectivity were found to be also influenced by the addition of promoters. It was shown that the activity increased by the addition of promoters attributed to the enhanced dispersion and reducibility that provided abundant active sites. The addition of alkali metal caused an increase in 1-alkene selectivity. Thus, the addition of alkali metal promoter was suggested to suppress the hydrogenation activity better than alkali-earth metal promoters. Moreover, the addition of Ca to the cobalt based catalyst greatly improved the diesel selectivity. However Ca promoted catalyst yield a higher amount of methane at 242 °C than the Na sample due to hydrogen spillover.

Acknowledgements

Financial supports from the Ministerio de Industria, Turismo y Comercio of Spain (CENIT-PiIBE project) and ELCOGAS S.A. are gratefully acknowledged.

References

[1] http://www.ipcc.ch/pdf/assessment-report/ar4/syr/ar4_syr.pdf.
[2] J. Fermoso, B. Arias, M.V. Gil, M.G. Plaza, C. Pevida, J.J. Pis, F. Rubiera, Bioresour. Technol. 101 (2010) 3230–3235.
[3] A. Demirbas, Prog. Energy Combust. Sci. 33 (2007) 1–18.
[4] M.J.A. Tijmensen, A.P.C. Faaij, C.N. Hamelinck, M.R.M. van Hardeveld, Biomass Bioenergy 23 (2002) 129–152.
[5] G.W. Huber, S. Iborra, A. Corma, Chem. Rev. 106 (2006) 4044–4098.
[6] K. Tomishige, M. Asadullah, K. Kunimori, Catal. Today 89 (2004) 389–403.
[7] S.T. Chaudhari, S.K. Bej, N.N. Bakhshi, A.K. Dalai, Energy Fuels 15 (2001) 736–742.
[8] S.Z. Li, S. Krishnamoorthy, A.W. Li, G.D. Meitzner, E. Iglesia, J. Catal. 206 (2002) 202–217.
[9] Ø. Borg, S. Eri, E.A. Blekkan, S. Stosater, H. Wigum, E. Rytter, A. Holmen, J. Catal. 248 (2007) 89–100.
[10] S.A. Hosseini, A. Taeb, F. Feyzi, F. Yaripour, Catal. Commun. 5 (2004) 137–143.
[11] J.L. Zhang, J.G. Chen, J. Ren, Y.H. Sun, Appl. Catal. A Gen. 243 (2003) 121–133.
[12] G. Jacobs, T.K. Das, Y.Q. Zhang, J.L. Li, G. Racoillet, B.H. Davis, Appl. Catal. A Gen. 233 (2002) 263–281.
[13] S.A. Hosseini, A. Taeb, F. Feyzi, Catal. Commun. 6 (2005) 233–240.
[14] T.K. Das, G. Jacobs, P.M. Patterson, W.A. Conner, J.L. Li, B.H. Davis, Fuel 82 (2003) 805–815.
[15] Y. Yang, H.-W. Xiang, Y.-Y. Xu, L. Bai, Y.-W. Li, Appl. Catal. A Gen. 266 (2004) 181–194.
[16] J. Yang, Y. Sun, Y. Tang, Y. Liu, H. Wang, L. Tian, H. Wang, Z. Zhang, H. Xiang, Y. Li, J. Mol. Catal. A Chem. 245 (2006) 26–36.
[17] J. Gaube, H.-F. Klein, Appl. Catal. A Gen. 350 (2008) 126–132.
[18] Y. Zhang, H. Xiong, K. Liew, J. Li, J. Mol. Catal. A Chem. 237 (2005) 172–181.
[19] A. Bao, K. Liew, J. Li, J. Mol. Catal. A Chem. 304 (2009) 47–51.
[20] D.A. Wesner, G. Linden, H.B. Bonzel, Appl. Surf. Sci. 26 (1986) 335–356.
[21] S. Eri, J.G. Goodwin Jr., G. Marcelin, T. Riis, US Patent 4,880,763, 1989.
[22] J.L. Li, N.J. Coville, Appl. Catal. A Gen. 181 (1999) 201–208.
[23] A.M. Hilmen, D. Schanke, K.F. Hanssen, A. Holmen, Appl. Catal. A Gen. 186 (1999) 169–188.
[24] M.L. Toebes, J.M.P. van Heeswijk, J.H. Bitter, A.J. Van Dillen, K.P. de Jong, Carbon 42 (2004) 307–315.
[25] C. Amorim, M.A. Keane, J. Chem. Technol. Biotechnol. 83 (2008) 662–672.
[26] K. van der Lee, A.J. van Dillen, J.H. Bitter, K.P. de Jong, J. Am. Chem. Soc. 127 (2005) 13573–13582.
[27] M.J. Ramos, A. Casas, L. Rodriguez, R. Romero, A. Pérez, Appl. Catal. A Gen. 346 (2008) 79–85.
[28] D. Schanke, S. Vada, E.A. Blekkan, A.M. Hilmen, A. Hoff, A. Holmen, J. Catal. 156 (1995) 85–95.
[29] R.D. Jones, C.H. Bartholomew, Appl. Catal. 39 (1988) 77–88.
[30] L.F. Liotta, G. Pantaleo, A. Macaluso, G. Di Carlo, G. Deganello, Appl. Catal. A Gen. 245 (2003) 167–177.
[31] J. Aguado, J.M. Escola, M.C. Castro, Micropor. Mesopor. Mater. 128 (2010) 48–55.
[32] W. Lv, Q. Qiu, F. Wang, S. Wei, B. Liu, Z. Luo, Ultrason. Sonochem. 17 (2010) 793–801.
[33] T. Horiuchi, H. Hidaka, T. Fukui, Y. Kubo, M. Horio, K. Suzuki, T. Mori, Appl. Catal. A Gen. 167 (1998) 195–202.
[34] S. Storsaeter, Ø. Borg, E.A. Blekkan, A. Holmen, J. Catal. 231 (2005) 405–419.
[35] K.S.W. Sing, D.H. Everett, R.A.W. Haul, L. Moscou, R.A. Pierotti, J. Rouquerol, T. Siemieniewska, Pure Appl. Chem. 57 (1985) 603–619.
[36] G. Jacobs, Y. Ji, B.H. Davis, D. Cronauer, A.J. Kropf, C.L. Marshall, Appl. Catal. A Gen. 333 (2007) 177–191.
[37] Ø. Borg, E.A. Blekkan, S. Eri, D. Akporiaye, B. Vigerust, E. Rytter, A. Holmen, Top. Catal. 45 (2007) 39–43.
[38] A. Lapidus, A. Krylova, V. Kazanskii, V. Borovkov, A. Zaitsev, J. Rathousky, A. Zukal, M. Janc̆álková, Appl. Catal. 73 (1991) 65–81.
[39] A.Y. Khodakov, W. Chu, P. Fongarland, Chem. Rev. 107 (2007) 1692–1744.
[40] W. Brockner, C. Ehrhardt, M. Gjikaj, Thermochim. Acta 456 (2007) 64–68.
[41] T.J. Gardner, G.L. Messing, Thermochim. Acta 78 (1984) 17–27.
[42] S. Gordon, C. Campbell, Differential Thermal Analysis of Inorganic Compounds Nitrates and Perchlorates of the Alkali and Alkaline Earth Groups and Their Subgroups, Analytical Chemistry 27 (1955) 1102–1109.
[43] L. González Tejuca, A.T. Bell, J.L.G. Fierro, M.A. Peña, Appl. Surf. Sci. 31 (1988) 301–316.
[44] M.E. Dry, G.J. Oosthuizen, J. Catal. 11 (1968) 18–24.
[45] R.B. Anderson, B. Seligman, J.F. Shultz, R. Kelly, M.A. Elliot, Ind. Eng. Chem. 44 (1952) 391–397.
[46] M.E. Dry, T. Shingles, L.J. Bischoff, G.J. Oosthuizen, J. Catal. 15 (1969) 190–199.
[47] A.R. Belamble, R. Oukaci, J.G. Goodwin Jr., J. Catal. 166 (1997) 8–15.
[48] Y. Wang, M. Noguchi, Y. Takahashi, Y. Ohtsuka, Catal. Today 68 (2001) 3–9.
[49] A.Y. Khodakov, R. Bechara, A. Griboval-Constant, Stud. Surf. Sci. Catal. 142 (2002) 1133–1140.
[50] F.E.M. Farias, F.G. Sales, F.A.N. Fernandes, J. Nat. Gas Chem. 17 (2008) 175–178.
[51] L. Tian, C-F. Huo, D-B. Cao, Y. Yang, J. Xu, B-S. Wu, H-W. Xiang, Y-Y. Xu, Y.-W. Li, J. Mol. Struct. Theochem. 941 (2010) 30–35.
[52] M. Trépanier, A. Tavasoli, A.K. Dalai, N. Abatzoglou, Appl. Catal. A Gen. 353 (2009) 193–202.
[53] D.O. Uner, M. Pruski, B.C. Gerstein, T.S. King, J. Catal. 146 (1994) 530–536.
[54] S.T. Hussain, M. Arif Nadeem, M. Mazhar, Catal. Commun. 9 (2008) 2048–2052.
[55] A. Nakhaeipour, S.M.K. Shahri, H.R. Bozorgzadeh, Y. Zamani, A. Tavasoli, M.A. Marvast, Appl. Catal. A Gen. 348 (2008) 201–208.
[56] M. Luo, R.J. O'Brien, S. Bao, B.H. Davis, Appl. Catal. A Gen. 239 (2003) 111–120.
[57] G. Zhao, C. Zhang, S. Qin, H. Xiang, H. Li, J. Mol. Catal. A Chem. 286 (2008) 137–142.
[58] A. Tavasoli, R.M. Malek Abbaslou, M. Trepanier, A.K. Dalai, Appl. Catal. A Gen. 345 (2008) 134–142.
[59] G. Jacobs, P.M. Patterson, T. Das, M. Luo, B.H. Davis, Appl. Catal. A Gen. 270 (2004) 65–76.
[60] R.C. Reuel, C.H. Bartholomew, J. Catal. 85 (1984) 63–77.
[61] A. Tavasoli, K. Sadaghiani, A. Nakhaeipour, M. Ghalbi Ahangari, Iran. J. Chem. Chem. Eng. 26 (2007) 1–9.
[62] R.J. Madon, E. Iglesia, J. Catal. 139 (1993) 576–590.
[63] M. Luo, B.H. Davis, Appl. Catal. A Gen. 246 (2003) 171–181.
[64] W. Ngantsoue-Hoc, Y. Zhang, R.J. O'Brien, M. Luo, B.H. Davis, Appl. Catal. A Gen. 236 (2002) 77–89.